Title

Aerosolized Silver Nanoparticles in the Rat Lung and Pulmonary Responses over Time

Journal

Toxicologic Pathology, 44(5)

ISSN

0192-6233

Authors

Silva, Rona M
Anderson, Donald S
Peake, Janice
et al.

Publication Date

2016-07-01

DOI

10.1177/0192623316629804

Peer reviewed

Published in final edited form as:

Toxicol Pathol. 2016 July ; 44(5): 673–686. doi:10.1177/0192623316629804.

Aerosolized Silver Nanoparticles in the Rat Lung and Pulmonary Responses over Time

Rona M. Silva[1], **Donald S. Anderson**[1], **Janice Peake**[1], **Patricia C. Edwards**[1], **Esther S. Patchin**[1], **Ting Guo**[2], **Terry Gordon**[3], **Lung Chi Chen**[3], **Xiaolin Sun**[1,4], **Laura S. Van Winkle**[1], and **Kent E. Pinkerton**[1]

[1]Center for Health and the Environment, University of California, Davis, California, USA

[2]Department of Chemistry, University of California, Davis, California, USA

[3]Department of Environmental Medicine, Langone Medical Center, New York University, Tuxedo, New York, USA

[4]Shandong University, School of Control Science and Engineering, Jinan, Shandong Province, China

Abstract

Silver nanoparticle (Ag NP) production methods are being developed and refined to produce more uniform Ag NPs through chemical reactions involving silver salt solutions, solvents, and capping agents to control particle formation. These chemical reactants are often present as contaminants and/or coatings on the Ag NPs, which could alter their interactions *in vivo*. To determine pulmonary effects of citrate-coated Ag NPs, Sprague-Dawley rats were exposed once nose-only to aerosolized Ag NPs (20 nm [C20] or 110 nm [C110] Ag NPs) for six hours. Bronchoalveolar lavage fluid (BALF) and lung tissues were obtained at 1, 7, 21, and 56 days post exposure for analyses. Inhalation of Ag NPs, versus citrate buffer control, produced significant inflammatory and cytotoxic responses that were measured in BALF cells and supernatant. At Day 7, total cells, protein, and lactate dehydrogenase were significantly elevated in BALF, and peak histopathology was noted after C20 or C110 exposure versus control. At Day 21, BALF PMNs and tissue inflammation was significantly greater after C20 versus C110 exposure. By Day 56, inflammation was resolved in Ag NP-exposed animals. Overall, results suggest delayed, short-lived inflammatory and cytotoxic effects following C20 or C110 inhalation and potential for greater responses following C20 exposure.

Keywords

pulmonary toxicity; inflammation; engineered nanomaterial; inhalation exposure

Correspondence: Dr. Kent E. Pinkerton, Center for Health and the Environment, University of California, One Shields Avenue, Davis, CA 95616. Tel: (530) 752-8334. kepinkerton@ucdavis.edu.

INTRODUCTION

Increased antimicrobial resistance, emergence of new pathogens, and resurgence of old infectious diseases necessitate novel solutions. Silver nanoparticles (Ag NPs) are being used to produce disinfectants in liquid (e.g., soaps and sprays), and solid (e.g., textiles and water treatments) forms due to their antimicrobial effects against a wide array of pathogens. Although use of nano silver is not new, our ability to produce it on a larger scale and incorporate it into a larger variety of matrices have expanded exponentially in recent years; thus, Ag NPs can be found in a myriad of consumer products (e.g., baby bottles, pesticides, dietary supplements), medical equipment/supplies (e.g., lab coats, catheters), and public spaces (e.g., subways) (Seltenrich, 2013).

Top-down production methods are often used to manufacture Ag NPs. These methods involve the use of physical processes (e.g., cutting, etching) which break down bulk silver precursor materials into isolated atoms. With this method, surface defects are common (U.S. Environmental Protection Agency, 2010). However, new bottom-up production methods are increasingly being developed and/or refined to manufacture more uniform and stable Ag NP suspensions through chemical reactions involving silver salt precursors (e.g., $AgNO_3$), solvents (e.g., ethylene glycol), reducing agents, and stabilizing/capping agents (e.g. citrate, or polyvinylpyrrolidone [PVP]) (Tolaymat *et al.*, 2010). These chemical reactants are often present as contaminants and/or coatings on the Ag NPs, which could alter their interactions *in vivo*. In the production of monodisperse Ag NP suspensions, citrate is a commonly used reducing and surface coating capping agent that can inhibit oxidative dissolution of Ag NPs (Huynh and Chen, 2011).

It is unclear whether and how Ag NPs and/or their coatings adversely affect human health. At least two occupational studies in Ag NP manufacturing plants have shown that the concentration of Ag NPs in the air increases during production (Park *et al.*, 2009, Lee *et al.*, 2012), which could increase the risk for inhalation exposure. Bolus intratracheal instillation or oropharyngeal aspiration exposure studies (Haberl *et al.*, 2013, Wang *et al.*, 2013) in rodents suggest that PVP- and citrate-coated Ag NPs are inflammatory and/or cytotoxic. Our laboratory (Silva *et al.*, 2015) has shown with 20 and 110 nm citrate- or PVP-coated Ag NPs that all Ag NP types produce a significant influx of inflammatory polymorphonuclear cells (PMNs) in bronchoalveolar lavage fluid (BALF) following an alternate exposure method, intratracheal instillation, at days 1, 7, and/or 21 post-exposure with 0.5 and/or 1.0 mg/kg body weight dose(s). Animals instilled with the highest dose had dead/dying cells at branch points along the main airway at post-exposure day 1 and centriacinar inflammation, including influx of PMNs, monocytes, and/or macrophages, at all time points. However, by post-exposure day 21, only animals instilled with 110 nm citrate- or PVP-coated Ag NPs (at 1.0 mg/kg body weight) exhibited significant BALF neutrophilia and marked cellular debris in alveolar airspaces.

Inhalation studies with uncoated Ag NPs suggest that they produce inflammation, allergic reactions, decrements in lung function, and/or DNA damage (Sung *et al.*, 2008, Sung *et al.*, 2009, Kwon *et al.*, 2012, Cho *et al.*, 2013, Chuang *et al.*, 2013, Su *et al.*, 2013, Song *et al.*, 2013, Braakhuis *et al.*, 2014) following acute, sub-chronic, and/or chronic exposures. In

contrast, numerous other inhalation studies suggest that uncoated Ag NPs produce no adverse (toxic) responses (Hyun *et al.*, 2008, Stebounova *et al.*, 2011, Sung *et al.*, 2011, Roberts *et al.*, 2013). For example, Stebounova and colleagues (2011) found that mice inhaling uncoated Ag NPs (5 ± 2 nm) at 3 mg/m^3, 4 hours/day, for 10 days showed minimal inflammatory or cytotoxic responses. Work by Roberts and colleagues (2013) with rats exposed to a wet aerosol of uncoated colloidal Ag NPs showed similar results. After 5 hours inhalation of a "low" (100 μg/m^3) or "high" (1000 μg/m^3) concentration of Ag NPs (mean aerodynamic diameter [MAD] = 33 or 39 nm, respectively) from a commercially available antimicrobial product, no acute toxic cardiopulmonary responses were noted. Although a study by Braakhuis and colleagues (2014) was completed using PVP-coated Ag NPs, the PVP was removed prior to exposure; therefore, our group is the first to investigate the pulmonary effects of coated Ag NPs.

The current study aimed to determine whether the responses noted previously upon intratracheal instillation (Silva *et al.*, 2015) and oropharyngeal aspiration (Wang *et al.*, 2013) were due to high Ag NP dose rates or physicochemical properties of the tested particles. The same batches of 20 and 110 nm citrate-coated Ag NPs (C20 and C110, respectively) tested by intratracheal instillation and oropharyngeal aspiration were used. The citrate-coated Ag NPs were chosen specifically because *in vitro* work by Wang and colleagues (2013) suggested that 20 nm Ag NPs exhibited faster dissolution and a higher ability to produce cellular toxicity and/or oxidative stress than 110 nm particles, irrespective of coating. In their study, citrate-coated Ag NPs produced greater and/or longer-lasting effects than PVP-coated ones due to a greater ability of PVP-coated Ag NPs to complex released Ag cations (Ag^+). Previous studies by our group, Anderson and colleagues (2014), using the same materials showed greater clearance of instilled PVP- versus citrate-coated Ag NPs. In accordance with findings by oropharyngeal aspiration (Wang *et al.*, 2013), we hypothesized that nose-only inhalation of C20 would produce greater acute cellular toxicity and neutrophilic inflammation than C110 and that C110 would produce mild sub-chronic pulmonary fibrosis.

Findings in the current study are considered in relation to a companion paper (Anderson *et al.*, 2015) reporting the Ag NP retention patterns for the same animals. Those results suggested that up to 56 days after nose-only inhalation of C20 or C110, silver persisted in lung tissues primarily at terminal bronchiole-alveolar duct junctions. In addition, at post-exposure days 21 and 56, silver from C20 persisted in BALF macrophages to a greater degree than C110.

MATERIALS AND METHODS

Physicochemical Characterization of Stock Ag Nanoparticles

Citrate-stabilized Ag NPs tested in the current study were purchased from nanoComposix, Inc. (San Diego, CA), from the BioPure™ line of materials and supplied by the National Institute of Environmental Health Sciences Centers for Nanotechnology Health Implications Research (NCNHIR) consortium. BioPure™ Ag NPs are extensively purified by nanoComposix, Inc. to remove residual reactants aside from those coating/capping the Ag NPs for stability (e.g., citrate); therefore, they are ideal for nanotoxicology and

environmental studies aimed at determining the effects of coated Ag NPs. Suspensions included 20 nm and 110 nm citrate-coated Ag NPs (lot numbers MGM1659 and MGM1662, respectively) that underwent initial physicochemical analysis by the National Characterization Laboratory (NCL). Primary size and morphology, hydrodynamic size and electrostatic potential, elemental and Ag^+ composition, and endotoxin content were determined using transmission electron microscopy (TEM), dynamic light scattering (DLS), inductively coupled plasma mass spectrometry (ICP-MS), and the Kinetic Turbidity and Gel-clot limulus amebocyte lysate (LAL) assays, respectively. Descriptions and results of these characterization methods have been presented previously (Wang *et al.*, 2013, Anderson *et al.*, 2014).

Aerosolized Ag NP size distribution, particle mass concentration, and silver concentration were determined as described (Anderson *et al.*, 2015) by TEM and a scanning mobility particle sizer (SMPS), gravimetric, and x-ray fluorescence (XRF) analyses, respectively.

Aerosol System and Inhalation Exposures

Preparation of the Ag NP and sham control suspensions and operation of the exposure system used for the inhalation studies have been described previously (Anderson *et al.*, 2015). Endotoxin free water (Fisher Scientific, Pittsburg, PA) was used to dilute trisodium citrate dihydrate powder (Sigma St. Louis, MO) to make a 2mM citrate buffer (pH = 7.5, sham control) of the same concentration as the suspended Ag NPs (1.0 mg/mL).

Ag NP suspension or sham control buffer was introduced via a BGI 6-jet Collison nebulizer (Waltham, MA) operated at 20 psi (6.9 kPa) for a manufacturer-specified output of 12 liters/minute over the exposure period. Utilization of the BGI nebulizer coupled to a downstream heater, diffusion dryers, and a Krypton-85 source (for charge neutralization) allowed for efficient delivery of a dry aerosol to the nose-only exposure chamber (Raabe *et al.*, 1973) with minimal aggregation of particles. The aerosolization and exposure system is shown in Figure 1 and is also described in Anderson *et al.,* (2015).

Food was removed from animal cages two hours prior to exposure. Each animal entered an exposure tube that was coupled at an open nose port to the exposure system. Rats were exposed to either nebulized Ag NPs in citrate buffer or citrate buffer alone for a single 6-hour period.

Animal Protocol

Male, twelve-week old Sprague-Dawley rats (Harlan Laboratories, Inc., Hayward, CA) were used for all experiments based on their extensive use in experimental studies and even temperament. Six animals per treatment group per time-point were randomly assigned (n = 72, including controls). Animals were maintained (Silva *et al.*, 2013), acclimated and exposed (Anderson *et al.*, 2015) in accordance with the UC Davis Institutional Animal Care and Use Committee. Animals were housed in pairs with enrichment objects and given access *ad libidum* to Laboratory Rodent Diet (Purina Mills, St Louis, MO). In the week prior to the scheduled exposure, animals were trained to enter and remain in the exposure tubes until released. Time in the tube increased incrementally up to 6 hours over the training to decrease confinement stress during the actual 6-hour inhalation exposure period.

After a one-time, 6-hr nose-only exposure to aerosolized C20, C110 or citrate buffer, animals were euthanized at 1, 7, 21, or 56 days post-exposure for collection of BALF and tissues. BALF was retrieved from lavaged right lungs, and separated into cellular and supernatant fractions for determination of cell counts and differentials (Anderson *et al.*, 2015) and same-day protein and lactate dehydrogenase (LDH) analyses, respectively. Isolated left lungs were fixed with 4% paraformaldehyde for subsequent sectioning and staining as previously described (Silva *et al.*, 2013). Hematoxylin and Eosin stains (H & E, Harris Hematoxylin, and Eosin Y Stain), were used to determine cellular infiltrates and epithelial abnormalities. Alcian Blue/Periodic Acid Schiff stain (AB/PAS) was used for verification of goblet (mucus) cell hyperplasia and/or changes in the types of mucosubstances being secreted in the airways. Stains were purchased from American MasterTech, Inc., Lodi, CA. Assessment of samples was performed blind. Semi-quantitative histological assessment of H & E slides was performed using an ordinal scoring system (Table 1) designed to distinguish the degree of lung inflammation in the H & E-stained tissue sections. Severity scores ranging from 0–3 were used, and severity was assessed by noting the most advanced grade present within the specific sample irrespective of its horizontal extent. Extent was defined as the horizontal distribution of the pathology, where a score of 0, 1, 2, or 3 meant none of the lung was involved, ≤ 1/3 involvement, > 1/3 to 1/2 involvement, or > 1/2 involvement, respectively. The overall score was defined as a combined assessment of severity and extent (overall score = severity × extent).

High resolution histopathology was enabled by examination of 1 μm lung sections embedded in araldite resin. Left lung lobes from two animals per treatment group (C20-, C110-, or citrate buffer-exposed) per time-point were fixed in Karnovsky's fixative and processed as previously described (Anderson *et al.*, 2014) to preserve ultrastructural cellular features.

Statistical Analysis

BALF data are presented as mean ± standard error of the mean (SEM). JMP 10.0.0 statistical software (Cary, NC) was used to perform analyses of variance (ANOVA), and post hoc Tukey's tests at a significance level of $p \leq 0.05$. Data were analyzed for deviations from the assumptions of ANOVA and transformed to meet the requirement of normality when needed. To address issues of skewness and/or kurtosis, BALF total cell and protein data were adjusted using $-1/x$, and $\log(x + 1)$ transformations, respectively, where "x" corresponded to an individual data point. Leptokurtic (peaked) BALF PMN data could not be corrected for normality. However, ANOVA was used because it tolerates violations to its normality assumption with only a small effect on Type I (false discovery) errors. To account for possible errors in the case of BALF PMNs, a stricter *p*-value of 0.01 was used.

Ordinal histopathology scores were also peaked. In this case, an ANOVA (p=0.01) was still preferable to multiple, separate non-parametric categorical analyses, which can introduce Type I and II errors and do not test the interactions between the independent variables. No outliers were identified for BALF of histopathology by box plots and/or Grubb's outlier tests.

RESULTS

Aerosol Characterization

Full descriptions of the generated aerosols have been reported previously (Anderson *et al.*, 2015). Silver concentrations averaged 7.2 ± 0.8 mg/m^3 and 5.3 ±1.0 mg/m^3 for C20 and C110 Ag NPs, respectively. According to cascade impactor measurements, 82% or 81% of C20 or C110 particles were ≤ 1.6 μm in diameter suggesting that the aerosolized particulates were sub-micron in size. Given the characterization data and a respiration minute volume for rats of approximately 0.21 L/min (Anderson *et al.*, 2015), silver deposition in the alveolar and tracheobronchial regions was estimated to be 69 and 17 μg, respectively, for C20 exposures, or 41 and 12 μg, respectively, for C110 exposures (Anderson *et al.*, 2015). Corresponding deposition in particle numbers would be approximately 1955 × 10^9 C20 or 7 × 10^9 C110 in the combined alveolar and tracheobronchial regions, respectively.

BALF Bioassays

Inhalation of Ag NPs (versus sham control) produced significant inflammatory and cytotoxic responses measured in BALF cell and supernatant data at 7 and/or 21 days post-exposure (Figure 2). Total BALF cells in Ag NP exposed animals was elevated at day 7 (Figure 2A), and this correlated to a concomitant increase in BALF protein (Figure 2B). BALF PMNs increased and peaked at 7 and 21 days after C20 exposure (Figure 2C) but not after inhalation of C110. LDH concentrations were elevated at Day 7 for both C20 and C110 groups versus citrate buffer groups (Figure 2D). Although inhalation of the citrate buffer alone appeared to produce some mild but significant inflammatory effects beyond that of C110 in a couple instances (Figures 2A–B), cumulatively, greater responses were observed due to Ag NP exposure. At day 7, BALF total cells, protein, and LDH were significantly elevated as a result of C20 or C110 exposure in contrast to sham control (Figures 2A, B, and D, respectively). These responses were also significantly higher than those noted on post-exposure days 1, 21, and/or 56, with responses returning to control levels by day 21. Significant influx of PMNs was noted only for C20 versus sham control exposed animals, and this response was significantly higher than that produced by C110 (Figure 2C). Protein concentrations at days 1 and 7 were also significantly higher in C20 than C110 exposed animals. No other significant differences were noted between C20 and C110 induced BALF inflammation or cytotoxicity. Overall, results suggested delayed, but short-lived inflammatory and cytotoxic effects due to C20 or C110 inhalation, with a potential for greater responses due to C20.

Changes in the lung parenchyma

Semi-quantitative scoring of H & E stained slides from post-exposure days 1 and 7 indicated mild but significant inflammation in animals exposed to C20 or C110 in contrast to the citrate control (Figures 3–5). Tissues recovered from animals exposed to citrate buffer exhibited occasional perivascular PMNs or macrophages in the alveolar airspaces at days 1, 7 and 21 with otherwise normal-looking lung parenchyma (Figures 4–7, panels A and B) during the time-course of this experiment. Conversely, inhalation of Ag NPs produced macrophages and/or neutrophils in the alveolar airspaces and, in the most severe cases, sloughing of the bronchiolar epithelium at day 1 (Figure 4, panels C, D and E, F). Peak

inflammation occurred at day 7 (Figure 3), when cellular exudate (Figure 5, panel D), enlarged macrophages (Figure 5, panels D and F), and some perivascular eosinophils (Figure 5, panels A, E, and F) were observed. During this time, particle agglomerates were still easily identified within the macrophages distributed throughout the alveolar spaces. By day 21 post-exposure, significant inflammation was observed only in response to C20 (versus control) (Figures 3 and 6). This is the only day in which significant histopathological differences were noted between C20 and C110 exposed animals (Figure 3). Results correlate with those reported by Anderson and colleagues (2015) showing greater persistence of C20 versus C110 in macrophages at day 21. By day 56, no significant degree of inflammation was detectable in Ag NP exposed animals (Figures 3). Due to the mild degree of inflammation noted by H & E (Figure 7) and lack of signs indicative of lung remodeling (e.g. thickening of the alveolar and/or bronchiolar epithelium), staining for collagen was not done.

Although tissues were stained with AB/PAS and analyzed for changes in the number of goblet cells and/or types of mucosubstances being secreted in the airways, no differences were observed irrespective of the treatment or post-exposure time-point.

Examination of araldite-embedded lung tissue sections revealed inflammation and sloughing of the airway epithelium along with increased presence of macrophages and enlarged Type II cells in the alveolar region at post Ag NP exposure day 1 (Figure 8). Ag NPs were clearly visible in macrophages, which were variably enlarged and/or vacuolated. At day 7, there was a clear septal wall response to Ag NPs. Alveolar Type II cells appeared more prominent in Ag NP vs citrate buffer exposed animals as did bronchiolar airway epithelia hypertrophy (Figure 9).

DISCUSSION

Most of the current research regarding the pulmonary health effects of Ag NPs has been done *in vitro*. Some more recent *in vivo* health studies are available, but of these, only a dozen use low dose rate inhalation as the method of Ag NP administration (Hyun *et al.*, 2008, Sung *et al.*, 2008, Sung *et al.*, 2009, Stebounova *et al.*, 2011, Sung *et al.*, 2011, Kwon *et al.*, 2012, Cho *et al.*, 2013, Chuang *et al.*, 2013, Roberts *et al.*, 2013, Song *et al.*, 2013, Su *et al.*, 2013, Braakhuis *et al.*, 2014). Route and method of delivery can have significant effects on physicochemical particle characteristics and physiological responses (U.S. Environmental Protection Agency, 2010) post exposure to NPs, and inflammation can be relatively less robust upon exposure to NPs at a low/steady rate versus a large bolus (Baisch *et al.*, 2014, Silva *et al.*, 2014). Considering only the published inhalation studies measuring pulmonary health endpoints, only two have been completed using nose-only exposure systems (Kwon *et al.*, 2012, Braakhuis *et al.*, 2014). This study, and its companion study on Ag NP clearance are the first to be completed using coated Ag NPs. Nose-only exposure systems can be considered the “gold standard” for measuring particle-size-dependent efficiencies (Phalen *et al.*, 2014). They are also ideal for examining pulmonary health effects by inhalation, specifically, because they limit exposure via other routes (e.g., oral by grooming), which may occur in whole-body inhalation chambers. Therefore, the current

study is important to the existing body of literature regarding the effects of inhaled Ag NPs in general, and, specifically, coated Ag NPs.

In this study, the aerosolized silver concentrations (7.2 ± 0.8 mg/m^3 and 5.3 ±1.0 mg/m^3 for C20 and C110, respectively) yielded estimated deposition in the alveolar and tracheobronchial regions (86 μg and 53 μg for C20 and C110, respectively) that overlaps with the instilled dose range previously reported (Anderson *et al.*, 2015, Silva *et al.*, 2015) and approximates worst-case exposure scenarios. The Occupational Safety and Health Administration (1988) and the European Commission (1993) set enforceable 8 hour time-weighted exposure limits for silver at 0.01 mg/m^3. Personal (breathing-level) occupational exposures (Lee *et al.*, 2011, 2012) to Ag NPs have been measured at well below these limits (2.43 μg/m^3, and 1.02 μg/m^3, respectively) in nano silver manufacturing plants. At the same time, area sampling yielded a maximal time-weighted average Ag NP concentration of 289 μg/m^3 of air. Particles ranged in aerodynamic diameter from 15 nm – 710.5 nm (Lee *et al.*, 2012). Workers were not directly exposed to the 289 μg/m^3 concentration in the study reported by Lee and colleagues (2012), but it can be used to correlate the inhaled doses herein to potentially high exposures that may occur in settings lacking proper exposure safeguards. Given the experimentally measured Ag NP concentration in the air and size range (Lee *et al.*, 2012), a (human lung) deposition fraction of approximately 10–40% (Geiser and Kreyling, 2010, Bair, 1995); a ventilation rate of 20 L/min (Galer *et al.*, 1992); and a human alveolar epithelium surface area of approximately 102 m^2 (Stone *et al.*, 1992), occupational exposure to 289 μg/m^3 Ag NPs would produce approximately 11, 55 and 218 μg Ag NPs/m^2 alveolar epithelium maximally after 1 day, 1 week, and 1 month, respectively. The alveolar epithelium of a Sprague-Dawley (SD) rat has a surface area of approximately 0.4 m^2 (Stone *et al.*, 1992), so alveolar deposition of 69 μg of C20 or 41 μg of C110, which was estimated for the current study, would result in 172.5 or 102.5 μg C20 or C110 Ag NPs/m^2 alveolar epithelium, respectively, for an average 350 g rat. These doses approximate human occupational exposures to Ag NPs between 2 weeks and 1 month in a light work environment.

Findings in this study suggest delayed peak and short-lived inflammatory and cytotoxic effects due to C20 or C110 inhalation (Figures 2 and 3) and potential for greater responses due to smaller Ag NPs (C20) (Figures 2–6 and 8). These latter results are consistent with a recent study (Braakhuis *et al.*, 2014) showing greater responses (increased PMNs and pro-inflammatory cytokines) to small versus large (15 versus 410 nm) Ag NPs after nose-only inhalation of similar mass concentrations (179 and 167 μg/m^3, respectively). In the current study, examination of BALF showed that at post-exposure day 7, total cell and PMN numbers were significantly greater in animals exposed to aerosolized Ag NPs versus citrate buffer (Figures 2A and C). Total cell numbers (Figure 2A) in C20 or C110 exposed animals peaked at day 7 and remained slightly but significantly elevated in contrast to day 1 through day 21 (C20 exposed) or day 56 (C110 exposed). Significantly higher numbers of BALF PMNs were also noted for C20 but not C110 exposed animals at day 7 versus all other days (Figure 2C). This peak in total BALF cells and/or PMNs correlated to a concomitant increase in the BALF concentration of LDH (Figure 2D), an intracellular enzyme, as well as tissue inflammation (Figure 3).

Presence of extracellular LDH in BALF supernatant is indicative of cell membrane permeability and cell necrosis. This LDH finding correlated with the visual confirmation of cellular exudate in the alveolar airspaces at post exposure day 7 for C20 and C110 exposures (Figure 5, panel D and Figure 9, panels C, E).

Anderson and colleagues (2015) noted that in spite of a lack of significant differences between Ag NP and citrate exposed animals, the number of BALF macrophages in Ag NP exposed animals was significantly elevated at days 21 and 56 in contrast to day 1. Therefore, high numbers of PMNs (C20-exposed animals only) and/or macrophages in Ag NP exposed animals contributed to the greater number of total cells noted at post-exposure days 21 and 56 versus day 1 (Figure 2A). Observations of delayed-onset and/or peak inflammation in BALF and tissues suggest that inhalation studies examining effects only up to 1 day post-exposure may miss peak responses (Kwon *et al.*, 2012), which in the current study occurred at day 7. Although histopathological scoring (Figure 3) showed that tissue inflammation peaked at day 7 for animals exposed to C20 or C110, only those exposed to C20 exhibited a concurrent influx of PMNs in contrast to control (Figure 2C). Given that histopathology scores considered the presence of macrophages, monocytes, and PMNs, and total BALF cell numbers were highest at day 7 post exposure to C20 or C110, results suggest that C20- but not C110-induced histopathology was driven to a large extent by PMN influx.

Significantly more BALF protein was noted upon inhalation of C20 versus C110 at post-exposure days 1 and 7 (Figure 2B). A similar pattern was noted for BALF PMNs on days 7 and 21 (Figure 2C) and histopathology at day 21 (Figure 3). Protein levels in the BALF often correlate with the degree of cellular inflammation in the lungs (Drent *et al.*, 1996). Differences in responses could be due to the far greater number of C20 (~1955×10^9 particles) delivered to the alveolar and tracheobronchial regions of the lungs versus C110 (~7×10^9 particles) and/or a relatively faster rate of Ag^+ leaching from inhaled parent C20.

The release rate of soluble or ionic silver (Ag^+) depends on multiple factors (e.g., Ag NP size and surface area, as well as ambient conditions) (Gliga *et al.*, 2014, Kim and Shin, 2014, Wang *et al.*, 2013, Hamilton *et al.*, 2014). Previous reports (Wang *et al.*, 2013, Hamilton *et al.*, 2014) testing the same Ag NPs used in this study (C20 and C110) suggest that small Ag NPs shed Ag^+ faster than large ones. Wang and colleagues (2013) showed by ICP-optical emission spectrometry (OES) that 20 nm citrate or PVP coated Ag NPs suspended in water or bronchial epithelial cell growth medium (BEGM) shed Ag^+ at significantly faster rates 0–24 hours post-incubation. Hamilton and colleagues (2014) showed by TEM imaging that intracellular (phagolysosomal) dissolution of 20 nm citrate or PVP coated Ag NPs was more rapid than that of similar 110 nm Ag NPs. *In vitro* exposure to C20 (but not C110) produced increased IL-1β, a measure of NLRP3-inflammasome activation, in several human and murine lung macrophage cell lines. NLRP3-inflammasome activation influences inflammation and apoptosis, and at post-exposure day 1 in the Hamilton study, NLRP3-inflammasome activation correlated with increased extracellular LDH and decreased cell viability (Hamilton *et al.*, 2014). Overall, the investigators' findings were consistent with Ag^+-mediated toxicity, which correlated with more robust inflammatory responses due to C20 inhalation (versus C110) in the current study (Figures 2B and C and Figure 3). Quantification of Ag NPs and other silver species in tissues may be

accomplished with single-particle ICP-MS (Gray *et al.*, 2013), atomic absorption spectrometry (Gliga *et al.*, 2014), or X-ray microprobe analysis (Gilbert *et al.*, 2012). Quantification is recommended for future Ag NP exposure studies because several researchers have shown that *in vitro* or acellular (media-based) Ag NP dissolution studies cannot duplicate the complexity and variability of the environ *in vivo* (Stebounova *et al.*, 2011, Scanlan *et al.*, 2013).

Collaborative research by Davidson and colleagues (2015) has been performed to better understand the dominant silver species in lung tissues upon inhalation of C20 and C110. X-ray absorption spectroscopy was performed at 0, 1, 3, and 7 days post-inhalation. Immediately after the 6-hour exposure (day 0), C20 were significantly modified in contrast to the largely unchanged C110. These findings correlate to those by Wang (2013), Zhang (2011), and their respective colleagues, who showed that C20 can undergo more rapid dissolution (into Ag^+) than C110. However, Davidson and colleagues (2015) also illustrated that over the 7 day post-exposure day period, changes in C110 were markedly greater than C20. Despite this, results suggested that metallic silver (not silver oxide or solvated silver cations) was most prevalent in the lung. The authors stated that if Ag^+ ions are responsible for toxic responses, such as reported here, then Ag^+ must be short lived. They speculated that Ag NPs undergo continuous cyclic evolution until all Ag species are cleared from the lung. In this process, transiently high concentrations of Ag^+ ions are produced locally (near parent Ag NPs). These ions are then reduced to metallic Ag atoms that are reformed into smaller Ag NPs. Their findings confirm *in vivo* differences in the chemical fates of inhaled C20 and C110 Ag NPs, which have been shown to produce distinct pulmonary responses (Anderson *et al.*, 2015)

Overall, it is unclear whether Ag NPs and/or their coatings will adversely affect human health. The purpose of this study was to better understand the health effects of inhaling citrate-coated Ag NPs with consideration to recovery over time and Ag NP size. No other studies to date have looked at pulmonary health effects after nose-only inhalation of coated Ag NPs. Thus, the data presented here are critical for future promulgation of laws, statutes, and regulations, creation and alteration of recommended exposure limits, and calculation of risks associated with Ag NP exposure.

Acknowledgments

Grant support [U01 ES020127 (UCD) and U01 ES0200126 (NYU)] and silver nanomaterials used in this study are procured, characterized and provided by the National Institute of Environmental Health Sciences Centers for Nanotechnology Health Implications Research (NCNHIR) Consortium.

All authors have read the final manuscript, and they wish to thank A. Castañeda, J. Claude, I. Espiritu, K. Johnson, and A. Pham for their assistance during the course of this study. Special thanks to Drs. N. Willits at the UC Davis Statistical Laboratory and S. Smiley-Jewell at the Center for Health and the Environment.

ABBREVIATIONS

AB/PAS	Alcian Blue/Periodic Acid Schiff stain
Ag NP(s)	silver nanoparticle(s)

$AgNO_3$	silver nitrate
ANOVA	analysis of variance
BALF	bronchoalveolar lavage fluid
BEGM	bronchial epithelial cell growth medium
C20/C110	20 nm/110 nm citrate-coated silver nanoparticles
DLS	dynamic light scattering
H & E	Harris Hematoxylin and Eosin Y Stain
ICP-MS	inductively-coupled plasma mass spectrometry
ICP-OES	inductively-coupled optical emission spectrometry
kPa	kilopascal
LAL	limulus amebocyte lysate
LDH	lactate dehydrogenase
MAD	mean aerodynamic diameter
NCL	National Characterization Laboratory
LOAEL	lowest observable adverse effect level
NOAEL	no observable adverse effect level
psi	pounds per square inch
PMNs	polymorphonuclear cells
PVP	polyvinylpyrrolidone
SEM	standard error of the mean
SMPS	scanning mobility particle sizer
TEM	transmission electron microscopy
XRF	x-ray fluorescence

References

Anderson DS, Silva RM, Lee D, Edwards PC, Sharmah A, Guo T, Pinkerton KE, Van Winkle LS. Persistence of Silver Nanoparticles in the Rat Lung: Influence of dose, size and chemical composition. Nanotoxicology. 2014:1–12.

Anderson DS, Patchin ES, Silva RM, Uyeminami DL, Sharmah A, Guo T, Das G, Brown JM, Shannahan J, Gordon T, Chen LC, Pinkerton KE, Winkle LSV. Influence of particle size on persistence and clearance of aerosolized silver nanoparticles in the rat lung. Toxicol Sci. 2015; 144:366–381. [PubMed: 25577195]

Bair WJ. The ICRP human respiratory-tract model for radiological protection. Radiat Prot Dosim. 1995; 60:307–310.

Baisch BL, Corson NM, Wade-Mercer P, Gelein R, Kennell AJ, Oberdorster G, Elder A. Equivalent titanium dioxide nanoparticle deposition by intratracheal instillation and whole body inhalation: the effect of dose rate on acute respiratory tract inflammation. Part Fibre Toxicol. 2014; 11:5. [PubMed: 24456852]

Braakhuis H, Gosens I, Krystek P, Boere J, Cassee F, Fokkens P, Post J, van Loveren H, Park M. Particle size dependent deposition and pulmonary inflammation after short-term inhalation of silver nanoparticles. Particle and Fibre Toxicology. 2014; 11:1–16. [PubMed: 24382024]

Cho H, Sung J, Song K, Kim J, Ji J, Lee J, Ryu H, Ahn K, Yu I. Genotoxicity of Silver Nanoparticles in Lung Cells of Sprague Dawley Rats after 12 Weeks of Inhalation Exposure. Toxics. 2013; 1:36–45.

Chuang HC, Hsiao TC, Wu CK, Chang HH, Lee CH, Chang CC, Cheng TJ, Taiwan CardioPulm Res Grp, T.C. Allergenicity and toxicology of inhaled silver nanoparticles in allergen-provocation mice models. Int J Nanomed. 2013; 8:4495–4506.

Davidson RA, Anderson DS, Van Winkle LS, Pinkerton KE, Guo T. Evolution of Silver Nanoparticles in the Rat Lung Investigated by X-ray Absorption Spectroscopy. The Journal of Physical Chemistry. 2015; 119:281–289. [PubMed: 25517690]

Drent M, Cobben NA, Henderson RF, Wouters EF, van Dieijen-Visser M. Usefulness of lactate dehydrogenase and its isoenzymes as indicators of lung damage or inflammation. The European respiratory journal. 1996; 9:1736–1742. [PubMed: 8866602]

European Commission. Recommendation from Scientific Expert Group on Occupational Exposure Limits for Metallic Silver. 1993. Retrieved Aug. 08, 2014 2014, from European Commission:ec.europa.eu/social/BlobServlet?docId=3857&langId=en

Galer DM, Leung HW, Sussman RG, Trzos RJ. Scientific and practical considerations for the development of occupational exposure limits (OELs) for chemical substances. Regulatory toxicology and pharmacology : RTP. 1992; 15:291–306. [PubMed: 1509122]

Geiser M, Kreyling W. Deposition and biokinetics of inhaled nanoparticles. Particle and Fibre Toxicology. 2010; 7:2. [PubMed: 20205860]

Gilbert B, Fakra SC, Xia T, Pokhrel S, Mädler L, Nel AE. The Fate of ZnO Nanoparticles Administered to Human Bronchial Epithelial Cells. ACS Nano. 2012; 6:4921–4930. [PubMed: 22646753]

Gliga AR, Skoglund S, Odnevall Wallinder I, Fadeel B, Karlsson HL. Size-dependent cytotoxicity of silver nanoparticles in human lung cells: the role of cellular uptake, agglomeration and Ag release. Part Fibre Toxicol. 2014; 11:11. [PubMed: 24529161]

Gray EP, Coleman JG, Bednar AJ, Kennedy AJ, Ranville JF, Higgins CP. Extraction and Analysis of Silver and Gold Nanoparticles from Biological Tissues Using Single Particle Inductively Coupled Plasma Mass Spectrometry. Environmental Science & Technology. 2013; 47:14315–14323. [PubMed: 24218983]

Haberl N, Hirn S, Wenk A, Diendorf J, Epple M, Johnston BD, Krombach F, Kreyling WG, Schleh C. Cytotoxic and proinflammatory effects of PVP-coated silver nanoparticles after intratracheal instillation in rats. Beilstein journal of nanotechnology. 2013; 4:933–940. [PubMed: 24455451]

Hamilton RF, Buckingham S, Holian A. The effect of size on Ag nanosphere toxicity in macrophage cell models and lung epithelial cell lines is dependent on particle dissolution. International journal of molecular sciences. 2014; 15:6815–6830. [PubMed: 24758926]

Huynh KA, Chen KL. Aggregation Kinetics of Citrate and Polyvinylpyrrolidone Coated Silver Nanoparticles in Monovalent and Divalent Electrolyte Solutions. Environmental Science & Technology. 2011; 45:5564–5571. [PubMed: 21630686]

Hyun JS, Lee BS, Ryu HY, Sung JH, Chung KH, Yu IJ. Effects of repeated silver nanoparticles exposure on the histological structure and mucins of nasal respiratory mucosa in rats. Toxicology Letters. 2008; 182:24–28. [PubMed: 18782608]

Kim MJ, Shin S. Toxic Effects of Silver Nanoparticles and Nanowires on Erythrocyte Rheology. Food and chemical toxicology : an international journal published for the British Industrial Biological Research Association. 2014; 67:80. [PubMed: 24534065]

Kwon JT, Minai-Tehrani A, Hwang SK, Kim JE, Shin JY, Yu KN, Chang SH, Kim DS, Kwon YT, Choi IJ, Cheong YH, Kim JS, Cho MH. Acute pulmonary toxicity and body distribution of inhaled metallic silver nanoparticles. Toxicological research. 2012; 28:25–31. [PubMed: 24278586]

Lee JH, Kwon M, Ji JH, Kang CS, Ahn KH, Han JH, Yu IJ. Exposure assessment of workplaces manufacturing nanosized TiO2 and silver. Inhal Toxicol. 2011; 23:226–236. [PubMed: 21456955]

Lee JH, Ahn K, Kim SM, Jeon KS, Lee JS, Yu IJ. Continuous 3-day exposure assessment of workplace manufacturing silver nanoparticles. Journal of Nanoparticle Research. 2012; 14:1134.

Occupational Safety and Health Administration. Silver, Metal and Soluble Compounds (as Ag). 1988. Retrieved Aug. 08, 2014 2014, from https://www.osha.gov/dts/chemicalsampling/data/CH_267300.html

Park J, Kwak BK, Bae E, Lee J, Kim Y, Choi K, Yi J. Characterization of exposure to silver nanoparticles in a manufacturing facility. Journal of Nanoparticle Research. 2009; 11:1705–1712.

Phalen, RF.; Mendez, LB.; Oldham, MJ. Inhalation Toxicology. CRC Press; Boca Raton, FL: 2014. p. 33487-2742.

Raabe OG, Bennick JE, Light ME, Hobbs CH, Thomas RL, Tillery MI. Improved apparatus for acute inhalation exposure of rodents to radioactive aerosols. Toxicol Appl Pharmacol. 1973; 26:264–273. [PubMed: 4751105]

Roberts JR, McKinney W, Kan H, Krajnak K, Frazer DG, Thomas TA, Waugh S, Kenyon A, MacCuspie RI, Hackley VA, Castranova V. Pulmonary and Cardiovascular Responses of Rats to Inhalation of Silver Nanoparticles. Journal of Toxicology and Environmental Health-Part a-Current Issues. 2013; 76:651–668.

Scanlan LD, Reed RB, Loguinov AV, Antczak P, Tagmount A, Aloni S, Nowinski DT, Luong P, Tran C, Karunaratne N, Pham D, Lin XX, Falciani F, Higgins CP, Ranville JF, Vulpe CD, Gilbert B. Silver Nanowire Exposure Results in Internalization and Toxicity to Daphnia magna. ACS Nano. 2013; 7:10681–10694. [PubMed: 24099093]

Seltenrich N. Nanosilver: weighing the risks and benefits. Environ Health Perspect. 2013; 121:A220–225. [PubMed: 23816826]

Silva RM, Teesy C, Franzi L, Weir A, Westerhoff P, Evans JE, Pinkerton KE. Biological response to nano-scale titanium dioxide (TiO2): role of particle dose, shape, and retention. Journal of toxicology and environmental health. Part A. 2013; 76:953–972. [PubMed: 24156719]

Silva RM, Anderson DS, Franzi LM, Peake JL, Edwards PC, Winkle LSV, Pinkerton KE. Pulmonary Effects of Ag NP Size, Coating, and Dose over Time upon Intratracheal Instillation. Toxicol Sci. 2015; 144:151–162. [PubMed: 25628415]

Song KS, Sung JH, Ji JH, Lee JH, Lee JS, Ryu HR, Lee JK, Chung YH, Park HM, Shin BS, Chang HK, Kelman B, Yu IJ. Recovery from silver-nanoparticle-exposure-induced lung inflammation and lung function changes in Sprague Dawley rats. Nanotoxicology. 2013; 7:169–180. [PubMed: 22264098]

Stebounova LV, Adamcakova-Dodd A, Kim JS, Park H, O'Shaughnessy PT, Grassian VH, Thorne PS. Nanosilver induces minimal lung toxicity or inflammation in a subacute murine inhalation model. Part Fibre Toxicol. 2011; 8:5. [PubMed: 21266073]

Stone KC, Mercer RR, Gehr P, Stockstill B, Crapo JD. Allometric relationships of cell numbers and size in the mammalian lung. Am J Respir Cell Mol Biol. 1992; 6:235–243. [PubMed: 1540387]

Su CL, Chen TT, Chang CC, Chuang KJ, Wu CK, Liu WT, Ho KF, Lee KY, Ho SC, Tseng HE, Chuang HC, Cheng TJ. Comparative proteomics of inhaled silver nanoparticles in healthy and allergen provoked mice. Int J Nanomedicine. 2013; 8:2783–2799. [PubMed: 23946650]

Sung JH, Ji JH, Yoon JU, Kim DS, Song MY, Jeong J, Han BS, Han JH, Chung YH, Kim J, Kim TS, Chang HK, Lee EJ, Lee JH, Yu IJ. Lung function changes in Sprague-Dawley rats after prolonged inhalation exposure to silver nanoparticles. Inhal Toxicol. 2008; 20:567–574. [PubMed: 18444009]

Sung JH, Ji JH, Park JD, Yoon JU, Kim DS, Jeon KS, Song MY, Jeong J, Han BS, Han JH, Chung YH, Chang HK, Lee JH, Cho MH, Kelman BJ, Yu IJ. Subchronic inhalation toxicity of silver nanoparticles. Toxicol Sci. 2009; 108:452–461. [PubMed: 19033393]

Sung JH, Ji JH, Song KS, Lee JH, Choi KH, Lee SH, Yu IJ. Acute inhalation toxicity of silver nanoparticles. Toxicology and industrial health. 2011; 27:149–154. [PubMed: 20870693]

Tolaymat TM, El Badawy AM, Genaidy A, Scheckel KG, Luxton TP, Suidan M. An evidence-based environmental perspective of manufactured silver nanoparticle in syntheses and applications: a systematic review and critical appraisal of peer-reviewed scientific papers. The Science of the total environment. 2010; 408:999–1006. [PubMed: 19945151]

U.S. Environmental Protection Agency. State of the Science Literature Review: Everything Nanosilver and More EPA/600/R-10/084. US Government Printing Office; Washington, DC: 2010.

Wang X, Ji Z, Chang CH, Zhang H, Wang M, Liao YP, Lin S, Meng H, Li R, Sun B, Winkle LV, Pinkerton KE, Zink JI, Xia T, Nel AE. Use of Coated Silver Nanoparticles to Understand the Relationship of Particle Dissolution and Bioavailability to Cell and Lung Toxicological Potential. Small (Weinheim an der Bergstrasse, Germany). 2013; 10:385–398.

Zhang W, Yao Y, Sullivan N, Chen Y. Modeling the Primary Size Effects of Citrate-Coated Silver Nanoparticles on Their Ion Release Kinetics. Environmental Science & Technology. 2011; 45:4422–4428. [PubMed: 21513312]

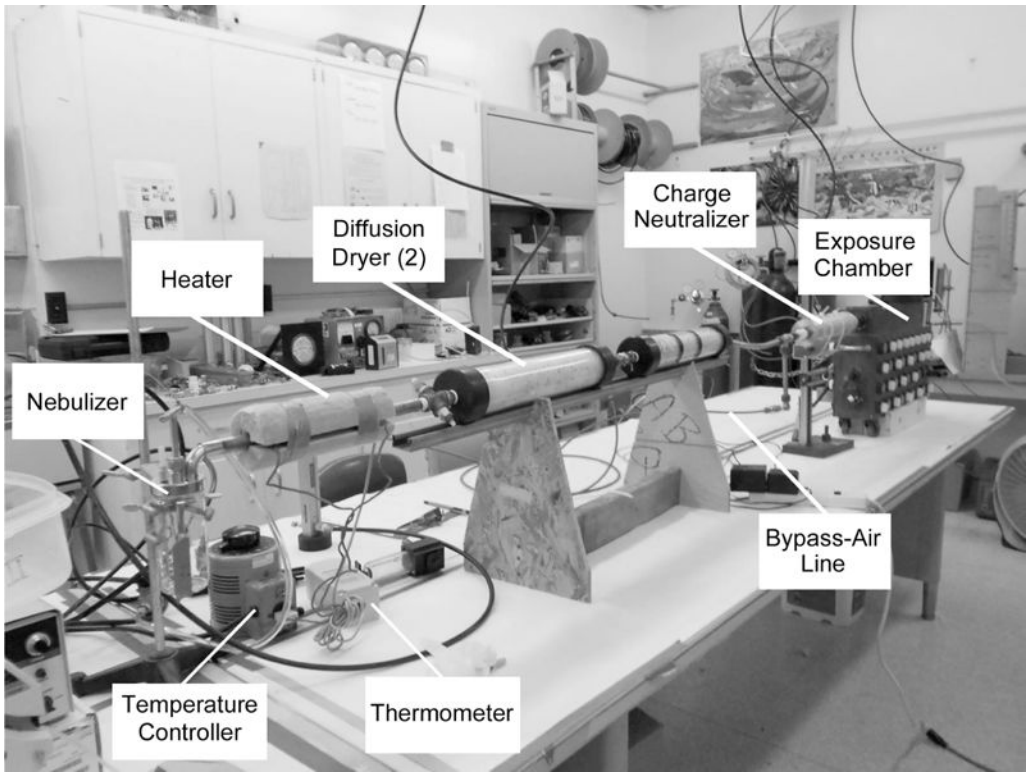

Figure 1.
Aerosolization and Exposure System

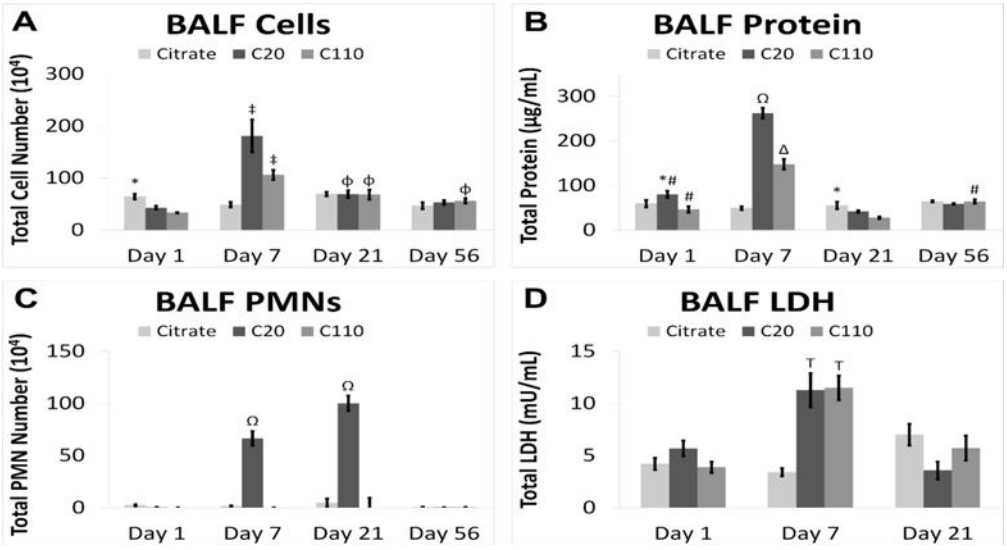

Figure 2. Peak BALF inflammation and cytotoxicity was observed 7 or 21 days post Ag NP exposure

Panels show (A) absolute numbers of total cells, (B) protein concentrations, (C) total PMNs, and (D) LDH on Days 1–56 post-inhalation of citrate buffer, C20, or C110. Results are from ANOVA considering the interaction between treatment and time. Ω = different from same day citrate and C110, as well as C20 at all other days ($p \leq 0.01$). Δ = different from citrate on the same day, and C110 at all other days ($p \leq 0.05$). T = different from same day citrate and from same treatment (C20 or C110) at days 1 & 21 ($p \leq 0.05$). ‡ = different from same day citrate and from same treatment (C20 or C110) at days 1 & 56 ($p \leq 0.05$). * = different from C110 (same day, $p \leq 0.05$). ϕ or # = different from day 1 or day 21, respectively (same treatment (C20 or C110), $p \leq 0.05$).

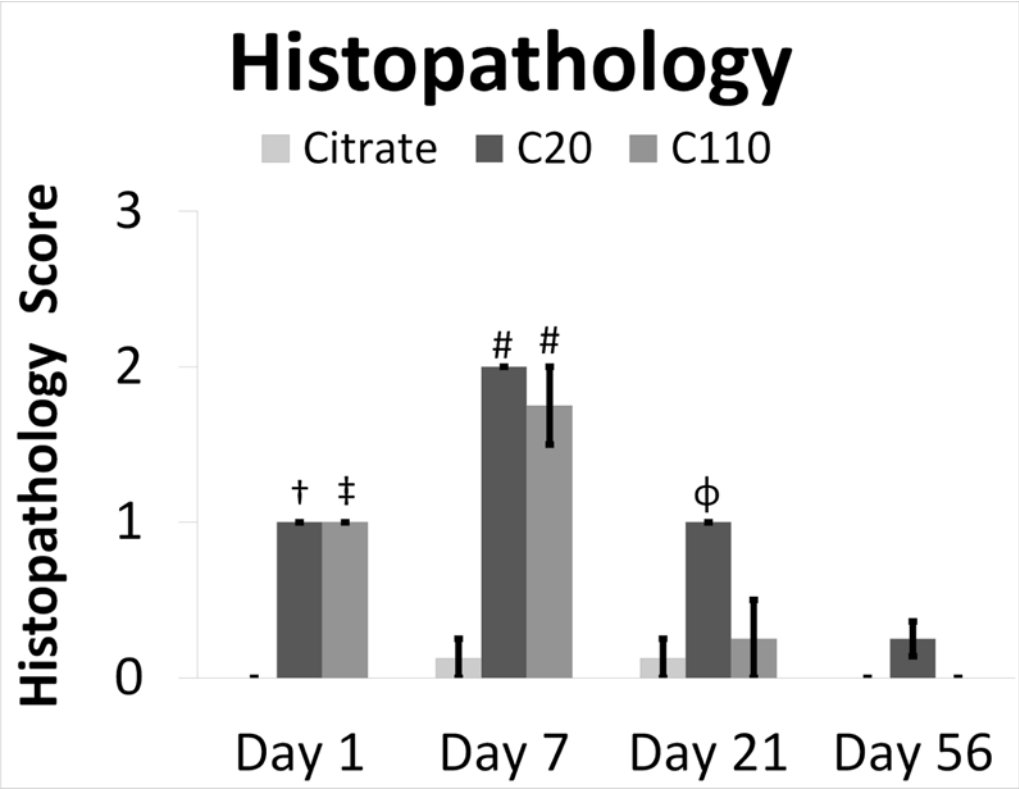

Figure 3. Ag NPs produce significant histopathology 1–21 Days Post Inhalation

Graphs show semi-quantitative histopathology scores for animal groups exposed to citrate buffer or Ag NPs by inhalation. Results are from an ANOVA considering the interaction of treatment and time post instillation. #, †, or ‡ = significantly different from (same day) citrate group ($p \leq 0.0001$) and all other days ($p \leq 0.0001$), days 21 and 56 ($p \leq 0.01$), or Day 56 only ($p \leq 0.01$), respectively. ϕ = different from (same day) citrate and C110 ($p \leq 0.01$) and Day 56 ($p \leq 0.001$).

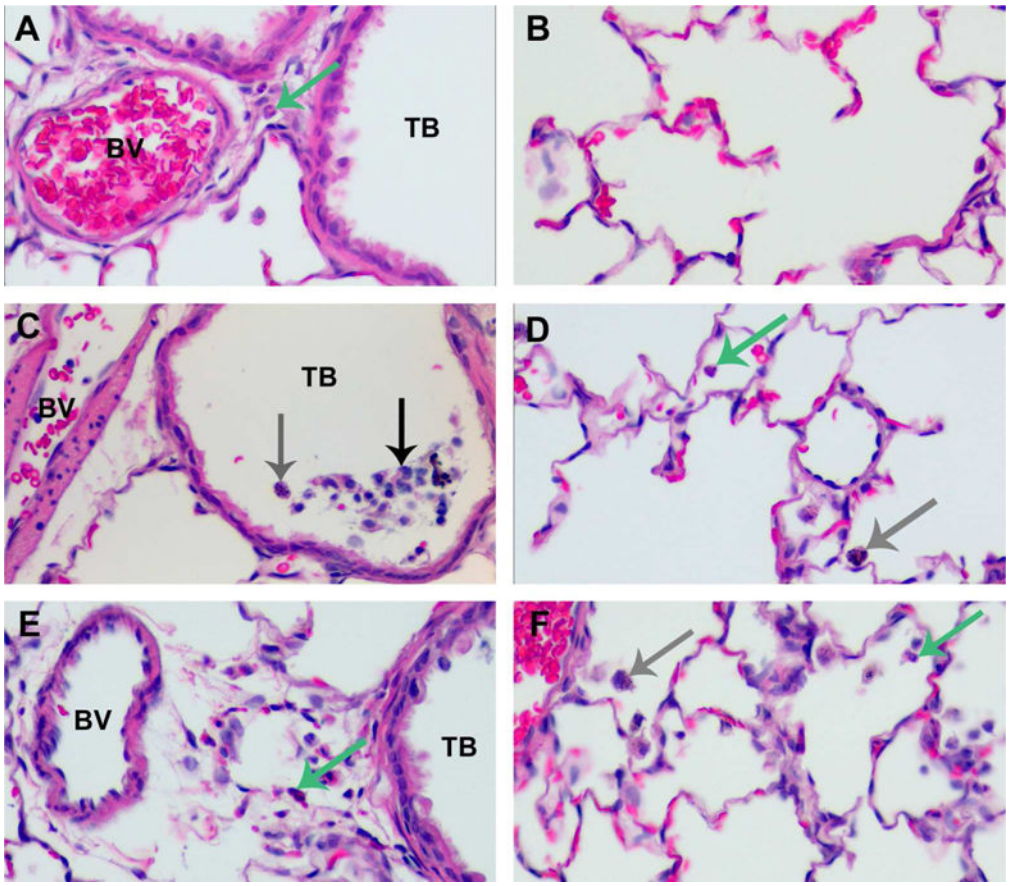

Figure 4. At post-inhalation Day 1, particle-laden macrophages and a mild influx of polymorphonuclear cells (PMNs) were noted in centriacinar regions

Panels are Brightfield microscopy images of typical responses in H & E-stained tissue sections from rats after inhalation of citrate buffer (sham control [A – B]), C20 (C – D), or C110 (E – F). Gray arrows indicate particle-laden macrophages. Green arrows indicate PMNs. Black arrow shows epithelial sloughing. Panels show cellular influx from blood vessels (BV) to sub-epithelial regions of the terminal bronchioles [(TB), A, C, E], or collecting in alveolar airspaces (B, D, F).

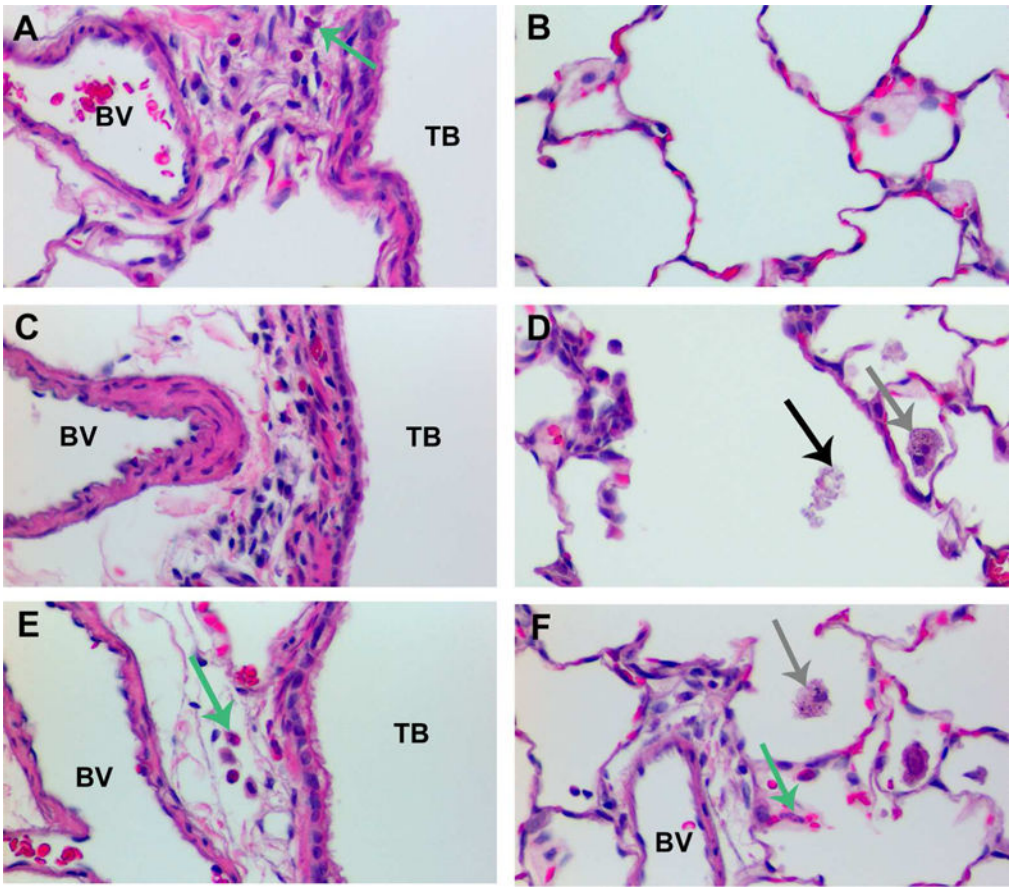

Figure 5. At post-inhalation Day 7, cellular exudate was prevalent in alveolar airspaces

Panels are Brightfield microscopy images of typical responses in H & E stained tissue sections from rats after inhalation of citrate buffer (sham control [A – B]), C20 (C – D), or C110 (E – F)]. Gray arrows indicate particle-laden macrophages. Green arrows indicate PMNs. Black arrow shows cellular debris. Panels show cellular influx from blood vessels (BV) to sub-epithelial regions of the terminal bronchioles ([TB]), A, C, E), or collecting in alveolar airspaces (B, D, F).

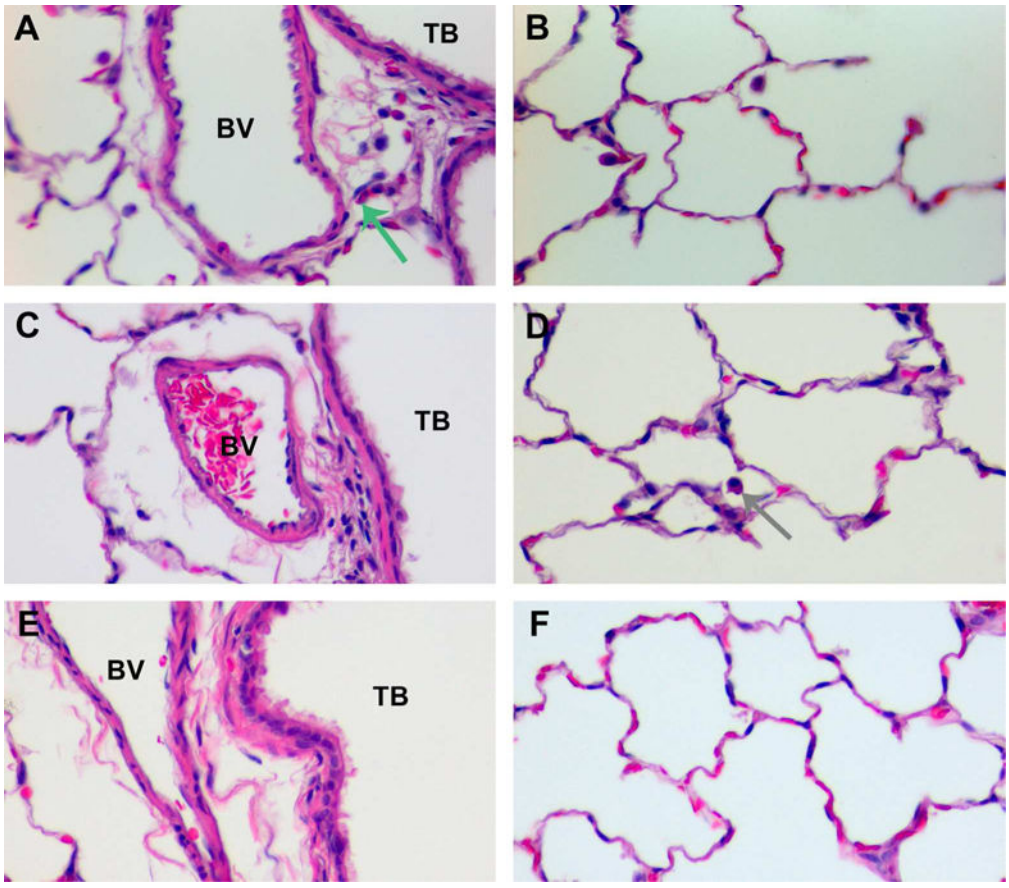

Figure 6. At post-inhalation Day 21, minimal cellular exudate and some cellular infiltrates were observed in lung tissue sections

Panels are Brightfield microscopy images of typical responses in H & E-stained tissue sections from rats after inhalation of citrate buffer (sham control [A – B]), C20 (C – D), or C110 (E – F). Green arrow indicates PMNs. Gray arrow indicates particle-laden macrophage. Panels show minimal (if any) cellular influx from blood vessels (BV) to sub-epithelial regions of the terminal bronchioles ([TB], A, C, E), or collecting in alveolar airspaces (B, D, F).

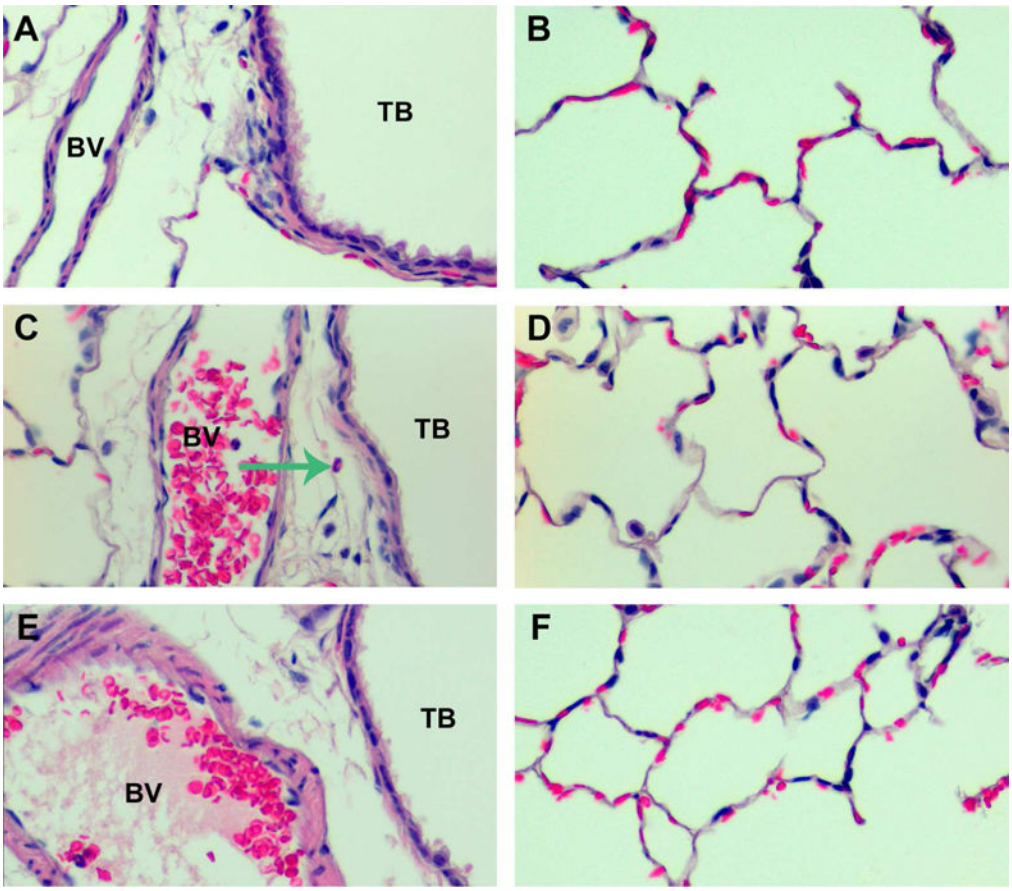

Figure 7. At post-exposure Day 56, inflammation was largely resolved

Panels are Brightfield microscopy images of typical responses in H & E stained tissue sections from rats after inhalation of citrate buffer (sham control [A – B]), C20 (middle - D), or C110 (E – F). Green arrow indicates PMNs. Panels show minimal (if any) cellular influx from blood vessels (BV) to sub-epithelial regions of the terminal bronchioles ([TB], A, C, E), or collecting in alveolar airspaces (B, D, F).

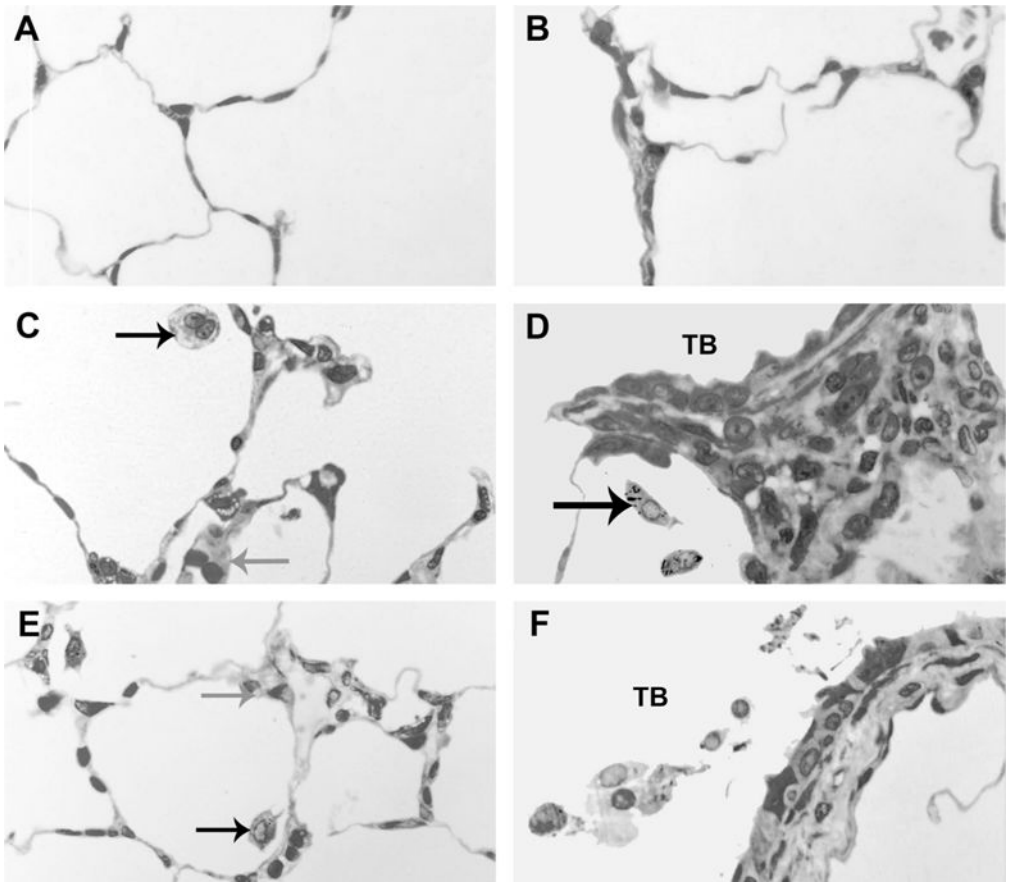

Figure 8. At post-inhalation Day 1, alveolar Type II cells appear enlarged (hypertrophied) with the thickened septal walls

Panels are Brightfield microscopy images of typical responses in araldite-embedded tissue sections from rats after inhalation of citrate buffer (sham control [A – B]), C20 (C – D), or C110 (E – F). Black arrows indicate enlarged and/or particle-laden macrophages. Gray arrows indicate thickened septal walls. Panels A, C, and E show the alveolar regions, while panels B, D, and F show the epithelial regions of the terminal bronchioles (TB).

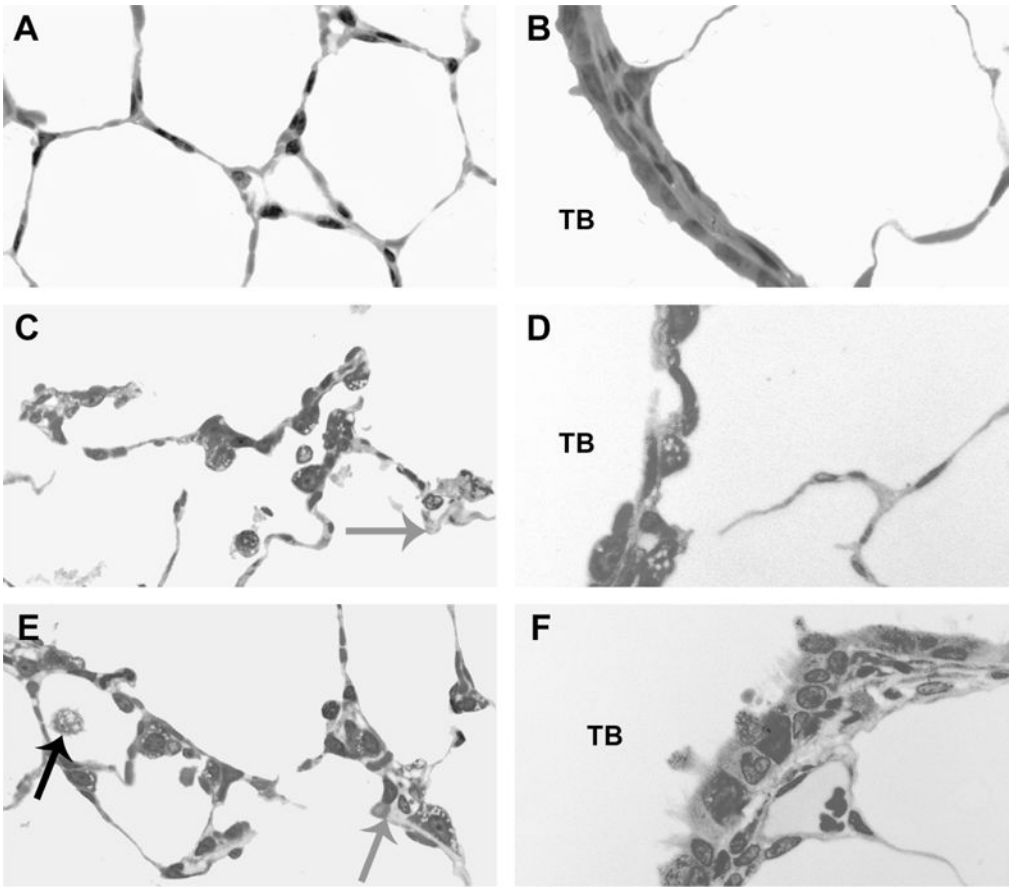

Figure 9. At post-inhalation Day 7, alveolar Type II cells appear to be undergoing mild hypertrophy, while the epithelia of the most distal airways also demonstrate visible hypertrophic changes, relative to controls

Panels are Brightfield microscopy images of typical responses in araldite-embedded tissue sections from rats after inhalation of citrate buffer (sham control [A – B]), C20 (C – D), or C110 (E – F). Black arrows indicate enlarged and/or particle-laden macrophages. Gray arrows indicate thickened septal walls. Panels A, C, and E show the alveolar regions, while panels B, D, and F show the epithelial regions of the terminal bronchioles (TB).

Table 1

Semi-quantitative histopathology severity scoring rubric.

Score	Description
0	Normal. Thin alveolar walls, with very few free macrophages and no inflammatory cells in the lumen. Respiratory epithelium 1 cell-layer thick. Normal smooth muscle and submucosal layers. Vascular endothelium may contain some influxing monocytes and a few inflammatory cells. No visible particle agglomerates. Little/no cells at the pleura.
1	PMNs present in perivascular cuff, airway submucosa and alveolar airspace. Influx of monocytes and macrophages into alveolar airspace and monocytes in perivascular cuff.
2	Presence of PMNs, macrophages, and monocytes in alveolar airspaces along with cellular debris (exudate). Influxing cells in the perivascular cuff and/or airway submucosa. Thickened alveolar walls.
3	Presence of PMNs and/or foamy and/or irregular macrophages (e.g. multi-nucleated, or exhibiting loss of membrane integrity) and cellular exudate in the airspaces. Thickened alveolar walls.